



LAWRENCE  
LIVERMORE  
NATIONAL  
LABORATORY

# Efficient Nanoporous Silicon Membranes for Integrated Microfluidic Separation and Sensing Systems

N. Ileri, S. E. Létant, J. Britten, H. Nguyen, C. Larson,  
S. Zaidi, A. Palazoglu, R. Faller, J. W. Tringe, P.  
Stroeve

April 22, 2009

Materials Research Society  
San Francisco, CA, United States  
April 13, 2009 through April 17, 2009

## **Disclaimer**

---

This document was prepared as an account of work sponsored by an agency of the United States government. Neither the United States government nor Lawrence Livermore National Security, LLC, nor any of their employees makes any warranty, expressed or implied, or assumes any legal liability or responsibility for the accuracy, completeness, or usefulness of any information, apparatus, product, or process disclosed, or represents that its use would not infringe privately owned rights. Reference herein to any specific commercial product, process, or service by trade name, trademark, manufacturer, or otherwise does not necessarily constitute or imply its endorsement, recommendation, or favoring by the United States government or Lawrence Livermore National Security, LLC. The views and opinions of authors expressed herein do not necessarily state or reflect those of the United States government or Lawrence Livermore National Security, LLC, and shall not be used for advertising or product endorsement purposes.

# Efficient Nanoporous Silicon Membranes for Integrated Microfluidic Separation and Sensing Systems

Nazar Ileri<sup>1,2</sup>, Sonia E. Létant<sup>2</sup>, Jerald Britten<sup>2</sup>, Hoang Nguyen<sup>2</sup>, Cindy Larson<sup>2</sup>, Saleem Zaidi<sup>3</sup>, Ahmet Palazoglu<sup>1</sup>, Roland Faller<sup>1</sup>, Joseph W. Tringe<sup>2</sup> and Pieter Stroeve<sup>1</sup>

<sup>1</sup>University of California, Davis, Davis, CA 95616, U.S.A.

<sup>2</sup>Lawrence Livermore National Laboratory, Livermore, CA 94550, U.S.A.

<sup>3</sup>Gratings, Inc., Albuquerque, NM 87107, U.S.A.

## ABSTRACT

Nanoporous devices constitute emerging platforms for selective molecule separation and sensing, with great potential for high throughput and economy in manufacturing and operation. Acting as mass transfer diodes similar to a solid-state device based on electron conduction, conical pores are shown to have superior performance characteristics compared to traditional cylindrical pores. Such phenomena, however, remain to be exploited for molecular separation. Here we present performance results from silicon membranes created by a new synthesis technique based on interferometric lithography. This method creates millimeter sized planar arrays of uniformly tapered nanopores in silicon with pore diameter 100 nm or smaller, ideally-suited for integration into a multi-scale microfluidic processing system. Molecular transport properties of these devices are compared against state-of-the-art polycarbonate track etched (PCTE) membranes. Mass transfer rates of up to fifteen-fold greater than commercial sieve technology are obtained. Complementary results from molecular dynamics simulations on molecular transport are reported.

## INTRODUCTION

Transport of biomolecules through nanopores is crucial in many biotechnological and biophysical processes [1]. Advances in protein screening, organic and inorganic molecular development, and sensing of toxins/viruses have enhanced the requirement for membranes with uniform pore size and a large dynamic range of biomolecule size selection (~1 nm to 1 $\mu$ m). However, the standard lithographic processes limit the production of membranes with near nanometer pore sizes over 1-100's of mm<sup>2</sup> areas needed by most applications. The majority of commercial membranes are made of organic polymers and fabricated by non-lithographic methods [2]. For example, PCTE membranes, produced by ion-track etching through polycarbonate films, have pore sizes in the range ~10 nm to ~ $\mu$ m. Although the scalability of these membranes is good, uniformity and flow rates are limited to  $\pm 20\%$  and  $< 0.1$  mL/min/cm<sup>2</sup> (for 10 nm diameter pores), respectively [3]. Other porous filters such as aluminum anodic oxide (AAO) and mesoporous silica have been created through anodic etching of Al [4, 5], and sol-gel processing [6], respectively. The pore dimensions vary between ~ 30-400 nm for anodic alumina and ~ 2-20 nm in sol-gel films, which limit their use due to lack of uniformity or scalability.

Membranes made of zeolites, on the other hand, have ultra-uniform pores, but only in the relatively narrow range of  $\sim 0.3\text{-}3$  nm [7].

Most current membranes have cylindrical pores which may present additional complications during filtration. Sieves with conical pores have been reported to exhibit dramatically higher transport rates compared to the analogous cylindrical pore membranes [8], but the current production methods are limited to polymeric membrane fabrication.

Here we present initial performance results of novel silicon membranes created by a new synthesis technique based on interferometric lithography. Silicon has a number of advantages as a filter material over the polymeric sieves including good mechanical, thermal and chemical stability, well controlled pore size and disinfection ability. Interferometric lithography enables definition of nanoscale features through interference of two laser beams incident on the same surface. With subsequent etching millimeter-sized planar arrays of uniformly tapered nanopores ( $\sim 100\text{nm}$ ) can be created in silicon with pore diameter 100 nm or smaller. Pyridine diffusion experiments are conducted to test the efficiency against commercial sieves.

## **THEORY AND EXPERIMENT**

For the fabrication of nanopore arrays, 4 inch, P-doped silicon-on-insulator SOI (100) wafers were used, with top silicon layer thickness  $\sim 380$  nm.  $\text{Si}_3\text{N}_4$  were deposited on both sides of the wafer to serve as Si etch mask. An antireflection coating (ARC) was used to suppress the standing wave formation resulting from substrate back-reflection. Next, positive resist was deposited on top of ARC and baked. The pattern was generated by large area interferometric lithography (IL) using a 413 nm Kr-ion laser as a light source. Pattern definition and ARC removal were followed by an electron-beam deposited Cr layer, and then lift-off of the resist film. Cr served as a mask for etching silicon nitride. After etching  $\text{Si}_3\text{N}_4$  down to the Si layer using an ion beam, a larger-scale pattern on the back side was created photolithographically to define the freestanding membrane areas, and the handle wafer was removed. Finally, pyramidal etch pits were etched on the front Si layer using a KOH solution, and the buried oxide layer was removed by vapor-phase HF etching.

To characterize the pores, the wafers were imaged after each processing step using atomic force microscopy (AFM) and scanning electron microscopy (SEM). AFM was conducted on a Nanoscope V5 and SEM with FEI 430 NanoSem Electron Beam Lithography System. To obtain statistical data on pore uniformity, images were analyzed with Scion Image Beta 4.0.3.

Mass transfer experiments were conducted using pyridine (HPLC grade, Aldrich Inc.) molecules. Commercial PCTE membranes with pore diameter in the  $\sim 100\text{nm}$  range (Poretics, Inc.) were used as received together with fabricated Si membranes. The membrane separated the diffusion cell into two compartments, reservoir and sink. The reservoir contained 1 mM aqueous solution of pyridine (30 mL), and the sink contained DI water (30 mL) without pyridine. The change of pyridine concentration in the sink compartment was measured by UV-visible light spectrophotometer (Varian, Cary 3) at 255nm.

For the molecular dynamics (MD) simulations, a solvent free coarse-grained model was used where proteins were treated as colloidal particles. The model was implemented by means of the ESPRESSO Molecular dynamics package [9]. Length, energy, and time were measured in units of  $\sigma$  (diameter of protein beads),  $\epsilon$  (cohesion potential depth between protein beads),  $\tau = \sigma (m/\epsilon)^{1/2}$  (m, bead mass), respectively. A mapping to real units can be established the following way: The diameter of a pore ( $100 \sigma$ ) corresponds to 100 nm leading to  $\sigma = 1$  nm. The temperature was chosen as  $k_B T = 1.0\epsilon$ . Since the thermal energy unit at room temperature is  $k_B T = 4.1 \times 10^{-21}$  J  $\approx 0.6$  kcal/mol (at  $T=298$  K).  $\epsilon$  is thus fixed at 0.6 kcal/mol. Finally, by using  $\tau = \sigma (m/\epsilon)^{1/2}$  and the known value for the protein mass,  $\tau$  was found to be 5.6ps. The time step was set to  $\delta t = 0.005 \tau$ . 30600 protein particles were placed in a  $100\sigma \times 100\sigma \times 200\sigma$  simulation box subject to periodic boundary conditions in all three dimensions. Temperature control was achieved by a dissipative particle dynamics (DPD) thermostat which ensures correct hydrodynamics. The friction constant was determined according to  $\Gamma = \tau^{-1}$ . The interactions between the filter and the protein beads as well as protein-protein beads were set to a purely repulsive Weeks-Chandler-Anderson potential [10], while there was no interaction between filter and beads. Visualization of simulation snapshots was performed with VMD [11].

## DISCUSSION

### Molecular Modeling

Three different pore geometries, i.e. cylindrical, conical, and pyramidal, were studied with large scale simulations (see Fig. 2). Higher diffusion rates were obtained with tapered geometries compared to cylindrical geometry for short simulation times (results not shown). This result is expected as the wall hindrance is much higher in cylindrical geometry in comparison with tapered pore geometry.

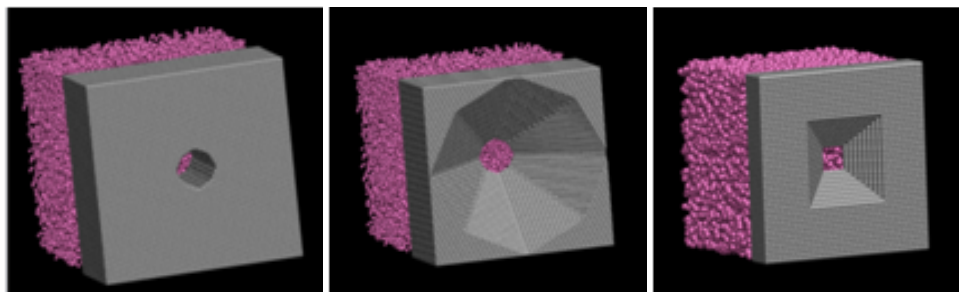


**Figure 2.** Simulation configurations for cylindrical, conical, pyramidal pores.

### Membrane Fabrication and Characterization

The initial pattern on the resist was defined by interferometric lithography (IL). IL exposures were strongly affected by conditions such as laser power, and thus exposure parameters had to be adjusted before each run. However, the technique exhibited good uniformity (see Table 1). Fig. 1 (b) shows a scanning electron microscopy image of a 833 nm period 2D photoresist pattern after exposing and developing.

After creating the pattern and etching the anti-reflective coating down to silicon nitride, a 50-nm Cr layer was deposited onto the surface and the resist layer was lifted-off (Fig. 1c). Non-uniformities increased after resist lift-off. The reason for increased non-uniformity was that the resist pillars were slightly wider at the bottom and narrower at the top. To circumvent this problem, the thickness of deposited Cr was increased (Fig 1d, 1e). Thicker Cr lead to higher uniformity results for the final silicon filter (Table 1), but the metal was then harder to remove. Since there was not a significant difference between 75 and 100 nm Cr thicknesses on uniformity results, 75 nm was selected as optimum. The silicon nitride served as a second etch mask for KOH etching on the front and back sides of the wafer since it exhibits improved mechanical stability and etch selectivity compared to the grown oxide layer.

The final features were created in silicon by KOH wet etching after  $\text{Si}_3\text{N}_4$  etch and handle wafer removal. Aqueous KOH solution etches Si in a highly anisotropic manner, and hence create near-perfect inverted pyramids. Since the silicon device thickness is  $\sim 380$  nm, the solution temperature was kept at room temperature in order to avoid fast etch rates. Moreover, the solution was stirred continuously to increase the diffusion rates of KOH into the pyramidal etch pits and improve the uniformity. Fig. 1f shows the cross-sectional SEM image of KOH etched patterns. KOH etching was followed by the final processing step, buried oxide removal with vapor-phase HF. Fig. 1g demonstrates top-down view of a complete membrane wafer.

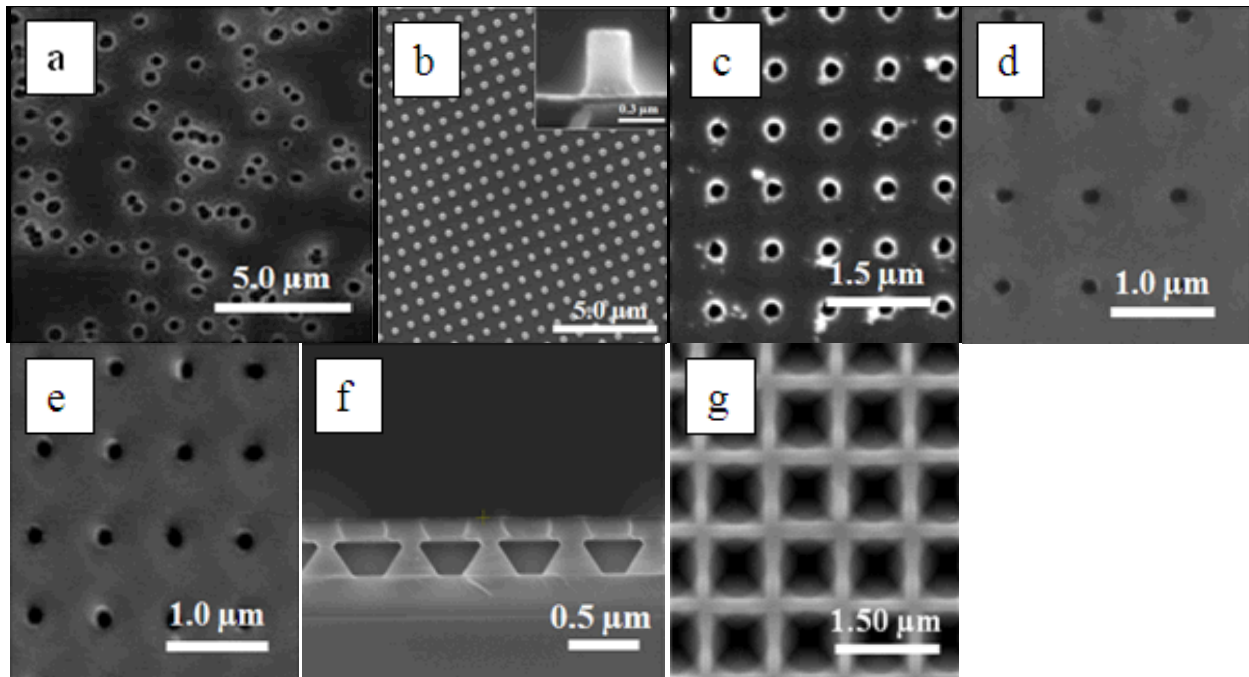


**Figure 1.** Scanning electron microscope images of (a) polycarbonate track etched (PCTE) membrane, (b) photoresist defined by interferometric lithography, (c) resist lift-off after 50nm Cr deposition, (d) resist lift-off after 75nm Cr deposition, (e) resist lift-off after 100nm Cr deposition, (f) V-grooves after front side KOH etching, (g) processed membrane wafer.

**Table 1.** Image analysis results comparing silicon membrane uniformity versus PCTE.

Pore/Membrane	PCTE	Pattern on resist	Silicon Filter
Diameter (nm)	326	$\leq 345$	100
Std. Dev. (nm)	249	69	48
Std. Error	0.76	0.20	0.48

### Transport Experiments

The efficiency of the fabricated filters in comparison to PCTE was investigated through a set of preliminary experiments. Pyridine was used in these experiments because the molecule diameter is significantly smaller ( $\sim 0.5$  nm) than the pore size ( $\sim 100$  nm), therefore allowing pure diffusion effect to be investigated. Table 2 shows mass transfer results for Si and PCTE membranes. Fifteen-fold higher fluxes obtained for Si membranes compared to state-of-the-art PCTE membrane with  $\sim 100$ nm pore diameter.

**Table 2.** Pyridine Flux through fabricated Si membranes versus commercially available PCTE membranes.

	PCTE	Si Membrane
Pore size (nm)	100	$\leq 100$
Membrane thickness (nm)	6000	280
Pore density (pores/cm <sup>2</sup> )	$6 \times 10^8$	$3 \times 10^8$
Pyridine flux (mole/cm <sup>2</sup> s)	$5.5 \times 10^{-10}$	$9.9 \times 10^{-9}$

### CONCLUSIONS

This study demonstrates the performance results of novel silicon membranes created by a new synthesis technique based on interferometric lithography. Highly uniform conical pores with pore diameter 100 nm or smaller were fabricated in silicon over millimeter-sized areas. Pyridine diffusion through silicon membranes was compared against the state-of-the-art polycarbonate track etched (PCTE) membranes. Pyridine transported through conical pores was found to be fifteen fold greater than through commercial filters. These observations were supported by molecular dynamics simulations showing higher diffusion rates for tapered pores compared to cylindrical pores. These newly created nano-filters could be integrated into a multi-scale microfluidic processing system and are expected to be useful for improving the selectivity, speed and efficiency of molecular separations for many biomedical and biodefense applications.

## ACKNOWLEDGMENTS

This work was partially supported the University of California System wide Biotechnology Research & Education Program GREAT Training grant 2007-03 and by LLNL LDRD. Special thanks to Harold Levie, Matthew Hoopes and Rodney Balhorn. Parts of this work were performed under the auspices of the U.S. Department of Energy by Lawrence Livermore National Laboratory under Contract DE-AC52-07NA27344.

## REFERENCES

1. C. Dekker, *Nature Nanotechnology*, vol. 2, pp. 209, 2007.
2. W. Chu, R. Chin, T. Huen, M. Ferrari, *J. Microelectromech. Syst.*, vol. 8, no. 1, pp. 34, 1999.
3. Sterilitech, "*Sterilitech Polycarbonate Track Etch (PCTE) Membranes*", <http://buyglassmicrofiber.com/>.
4. A. P. Li, F. Muller, A. Birner, K. Nielsch, and U. Gosele, *J. Appl. Phys.*, vol. 84, pp. 6023, 1998.
5. H. Masuda and K. Fukuda, *Science*, vol. 268, pp. 1466, 1995.
6. W. Chen, W. Cai, L. Zhang, G. Wang, and L. Zhang, *J. Coll. Interf. Sci.*, vol. 238, pp. 291, 2001.
7. I. Lenntech, "*Regenerative adsorption zeolite*", <http://www.lenntech.com/>.
8. N. Li, S. Yu, C.C. Harrell, C. R. Martin, *Anal. Chem.*, vol.76, pp. 2025, 2004.
9. H.J. Limabach, A. Arnold, B. A. Mann, *C. Holm, Comput. Phys. Commun.*, vol 174, pp. 702, 2006.
10. J. D. Weeks, D. Chandler, H. C. Anderson, *J. Chem, Phys.*, vol 54, pp. 5237, 1971.
11. W. Humphery, A. Dalke, K. Schulten, *J. Mol. Graph.*, vol. 14, pp. 33, 1996.